Original Article

MOLECULAR METABOLISM

Increased mitochondrial fusion via systemic OPA1 overexpression promotes dyslipidemia and atherosclerosis in LDLR deficient mice

Lorenzo Da Dalt[1], Francesca Fantini[1], Giulia Giancane[1], Annalisa Moregola[1], Silvia Roda[1], Monika Svecla[1], Silvia Pedretti[1,6], Giovanni Battista Vingiani[1], Jiangming Sun[2], Andreas Edsfeldt[2,3,4], Isabel Goncalves[2,3], Patrizia Uboldi[1], Elena Donetti[5], Andrea Baragetti[1], Nico Mitro[1,6], Luca Scorrano[7,8], Giuseppe Danilo Norata[1,*]

ABSTRACT

Objective: Mitochondria are involved in cellular metabolism, energy production, calcium homeostasis, and the synthesis of sterols and bile acids (BAs). Emerging evidence suggests that mitochondrial dynamics including biogenesis, fusion, fission, and mitophagy critically influence cardiometabolic diseases, yet their role in atherogenesis remain poorly understood. Mitochondrial fusion ensures metabolic flexibility and stress adaptation, processes highly relevant to lipid handling and vascular cell plasticity. OPA1, a key regulator of inner mitochondrial membrane fusion, has been implicated in metabolic remodeling and cellular stress responses. We therefore investigated whether modulation of OPA1 expression affects lipid homeostasis and plaque formation in LDL receptor-deficient (LDLR KO) mice and in human carotid atherosclerosis.
Methods: OPA1^{TG}/LDLR KO and OPA1$^{\Delta Hep}$/LDLR KO were fed with a Western-type diet (WTD) for 12 weeks. The development of atherosclerosis was compared to that of LDLR KO mice. In humans, the impact of OPA1 was investigated in asymptomatic and symptomatic subjects from the Carotid Plaque Imaging Project (CPIP) biobank.
Results: OPA1^{TG}/LDLR KO mice showed a significant increase in plasma cholesterol levels mainly in VLDL and LDL fractions. OPA1^{TG}/LDLR KO display a reduction of unconjugated bile acids and higher percentage of conjugated bile acids leading to an increased lipid adsorption. This phenotype was associated with increased atherosclerosis in the aortic root. OPA1 overexpression also resulted in an altered vascular smooth muscle cell (VSMC) cellular metabolism and differentiation, promoting a shift from a contractile/synthetic phenotype toward a more proliferative and metabolically active state. Concordantly, the deletion of OPA1 in hepatocytes improved systemic lipoprotein metabolism protecting from atherosclerosis. Concordantly in humans, plaque OPA1 mRNA levels are associated with metabolic and smooth muscle cell related pathways.
Conclusions: Mitochondrial fusion mediated by OPA1 plays a key role in atherosclerosis by affecting lipoprotein metabolism and vascular smooth muscle cell biology.
© 2025 The Author(s). Published by Elsevier GmbH. This is an open access article under the CC BY-NC-ND license (http://creativecommons.org/licenses/by-nc-nd/4.0/).

Keywords OPA1; Liver; Lipoprotein; Atherosclerosis; VSMCs

1. INTRODUCTION

Atherosclerosis is a chronic inflammatory disease characterized by the progressive accumulation of lipids and inflammatory cells within the arterial wall. It is one of the leading causes of cardiovascular disease, including heart attacks and strokes, and remains a significant global health concern [1]. Risk factors of atherosclerosis can be divided in two categories: modifiable (associated with lifestyle and environment) and unmodifiable (genetic variants, age and gender). While the role of lipoprotein metabolism in atherosclerosis has been extensively studied, emerging evidence suggests that metabolic mitochondrial impairment and altered cellular metabolism within atherosclerotic resident cells play a crucial role in the development and progression of the disease [2].
Mitochondria are the energetic suppliers of the cell, responsible for generating adenosine triphosphate (ATP) through oxidative phosphorylation. In the liver, beyond their role as crucial organelles for cellular energy balance, they can affect systemic lipid and lipoprotein metabolism [3]. We previously showed that decreased inner mitochondrial membrane fusion limits mitochondrial interaction with the endoplasmic reticulum and the peroxisomes, that affects cholesterol trafficking and the generation of conjugated bile acids, which in turn might affect the development of obesity and metabolic syndrome [4].

[1]Department of Pharmacological and Biomolecular Sciences "Rodolfo Paoletti", Università degli Studi di Milano, Milan, Italy [2]Department of Clinical Sciences Malmö, Lund University, Sweden [3]Department of Cardiology, Skåne University Hospital, Malmö, Sweden [4]Wallenberg Centre for Molecular Medicine, Lund University, Sweden [5]Department of Biomedical Science for Health, Universita` degli Studi di Milano, Milan, Italy [6]Department of Experimental Oncology, IEO, European Institute of Oncology IRCCS, Milan, Italy [7]Department of Biology, University of Padova, Padova, Italy [8]Veneto Institute of Molecular Medicine, Padova, Italy

*Corresponding author. E-mail: Danilo.Norata@unimi.it (G.D. Norata).

Received July 24, 2025 • Revision received September 11, 2025 • Accepted September 17, 2025 • Available online 22 September 2025

https://doi.org/10.1016/j.molmet.2025.102256

 © 2025 The Author(s). Published by Elsevier GmbH. This is an open access article under the CC BY-NC-ND license (http://creativecommons.org/licenses/by-nc-nd/4.0/).

Beyond a potential role in systemic metabolism, mitochondrial dynamism is critical also for vascular cell biology. Indeed, within the atherosclerotic lesion, various resident cells, such as vascular smooth muscle cells (VSMCs), endothelial cells and macrophages, undergo metabolic alterations that promote disease progression [5]. Accumulating evidence suggests that mitochondrial dysfunction in these cells contributes to altered lipid metabolism, inflammatory responses, and plaque instability [6]. Smooth muscle cells (SMCs) within the arterial wall exhibit metabolic alterations during atherosclerosis that are associated with a switch from a contractile to a synthetic phenotype, thus promoting their migration and proliferation within the lesion [7]. This phenotypic transition is associated with enhanced lipid uptake, increased production of extracellular matrix components, and the formation of a fibrous cap, characteristic of advanced plaques [8]. Understanding the impact of mitochondrial dynamism on atherosclerosis is crucial to design novel therapeutic strategies aimed at modulating lipid disposal, inflammation, and plaque stability for the treatment of atherosclerotic cardiovascular disease.

In this study, we aim at investigating the interconnection between mitochondrial plasticity, lipoprotein metabolism and the development of atherosclerosis.

We recently described that Optic Atrophy 1 (OPA1) deficiency modulates lipids and lipoprotein metabolism by controlling bile acid production and dietary lipid absorption [4]. Here we investigate whether OPA1 overexpression affects lipid and lipoprotein metabolism and how this could impact atherosclerosis development and vascular cell biology in LDL receptor deficient mice. We also investigated the features of human carotid plaques presenting an increased expression of OPA1.

Our data show that Opa1 overexpression leads to a significant increase in lipid uptake from the diet leading to an increase in atherogenic lipoproteins. Interestingly, higher levels of Opa1 in human atherosclerotic plaques are associated with changes in plaque features and correlates with enhanced plaque development. Our results underscore a critical role for OPA1 in regulating lipid metabolism and atherogenesis.

2. METHODS

2.1. Mice

We generated two new mice models on LDLR KO background that overexpress the human form of OPA1 (hOPA1) (OPA1^{TG}/LDLR KO) or that lacks Optic Atrophy 1 (OPA1) selectively in hepatocytes (OPA1$^{\Delta Hep}$/LDLR KO). OPA1^{TG}/LDLR KO mice were generated by crossing female OPA1 ^{TG} with LDLR KO male for 10 generation (Sup. Figure 1A). OPA1$^{\Delta Hep}$/LDLR KO were generated by crossing Opa1 flox/flox mice bearing Cre recombinase expression under the control of Albumin promoter (Alb-CRE) with LDLR KO mice for more than 10 generation to obtain OPA1 flox/flox-Cre+/LDLR KO (OPA1$^{\Delta Hep}$/LDLR KO) and controls Opa1 flox/flox/LDR KO (presented hereafter as OPA1$^{fl/fl}$ - LDLR KO) mice. Animals were housed three-four per cage, with a 12-h light/dark cycle in a temperature-controlled environment (20 $\pm$ 2 °C, 50 $\pm$ 5% relative humidity) and with free access to food and water. 8-weeks-old male littermates were fed with high cholesterol diet (western-type diet—WTD, E15775-34 ssniff® Spezialdiaten GmbH, DE) for 12weeks. Mice were sacrificed after overnight fasting, by CO_2 inhalation and blood was collected by intracardiac puncture followed by aorta, heart, mediastinal lymph nodes and spleen collection. All animal procedures were performed in accordance with the guidelines from directive 2010/63/EU of the European Parliament on the protection of animals used for scientific purposes and were approved by the pertinent Ethical Committees (Autorizzazione Ministeriale 384/2019-PR, 92/2020, 240/2021 and 565/2022).

2.2. Plasma triglyceride and cholesterol quantification

After overnight fasting, blood was collected in EDTA, and plasma was then separated by centrifugation at 1800 rcf for 10 min. Plasma levels of cholesterol and triglyceride (TG) were determined by a colorimetric enzymatic technique (ABX Pentra, HORIBA Medical). Cholesterol and TG content in lipoprotein fractions was performed following size fractionation of lipoproteins by fast performance liquid chromatography (FPLC) using a Superose 6 column (GE Healthcare, Chicago, IL, USA) on an NGCTM chromatography system FPLC (BioRad laboratories Inc., Hercules, CA, USA) with an eluent solution consisting of 0.15 M NaCl pH 7.2 + 0.01% EDTA + 0.02% Sodium azide. Aa pool of plasma from 6 mice per group was processed for FPLC analysis. The system was kept at a constant flow rate of 0.25 mL/min 0.5 mL of each fraction was collected and cholesterol and triglycerides concentrations were analyzed as previously described.

2.3. Quantification of hepatic bile acids content

Liver bile acids were extracted and quantified as previously described [4]. Briefly, 10 mg of liver were homogenized with 1 mL of extracting solution (Methanol/Acetonitrile, 1:1, v/v) using tissue lyser (max power, 1 min), incubated for 15 min at 37 °C and centrifuged at 16,000$\times g$ for 10 min at 20 °C. The samples were transferred into 96 well-plate auto-sampler for LC-MS/MS analysis. The analyses were performed on an API4000 triple quadrupole mass spectrometer (AB Sciex) coupled with an HPLC system (Agilent) and CTC PAL HTS autosampler (PAL System). The mobile phases were (A) 10 mM NH_4Ac and 0.015% formic acid in water, (B) 10 mM NH_4Ac and 0.015% formic acid in Acetonitrile/Methanol/Water (65/30/5). The Hypersil GOLD column C18 (100 mm $\times$ 3 mm, 3 μm) was maintained at 50 °C. The injection volume was 10 μl, and the injector needle was washed with Methanol/Water 1:1 (v/v). The mass spectrometer was operated in negative ion mode and selective ion monitoring (SIM)/SIM mode, and peaks were evaluated using Multiquant software (AB Sciex). Quantitative data were normalized on total liver protein content determined by Bradford. Presented data are expressed as ng/mg of liver protein.

2.4. Oral lipid tolerance test

The procedure was performed on overnight fasted animals fed WTD. After fasting, basal plasma triglycerides levels were measured, subsequently, mice received an oral gavage of oil (250 μl of EVO oil for mouse). Following the bolus, plasma was collected in EDTA tubes and plasma triglyceride levels were measured as previously described 1, 2, and 4 h after the gavage.

2.5. Circulating biomarkers profile

Plasma was collected on EDTA and immediately frozen. Plasma levels of Aspartate Aminotransferase (AST), Alanine Aminotransferase (ALT), Creatinine and Blood Urea Nitrogen (BUN) were measured with commercially available kits run on automatic analyzer (Randox, Crumlin, Ireland), (for ALT Cat#AL8006; for Creatinine Cat#CR8316 for AST Cat#AS8306 and for BUN Cat#UR446). Data from plasmatic enzyme measurement were obtained from 3 technical replicates of 6 biological replicates.

2.6. Glucose tolerance test (GTT)

GTT was performed after 12 weeks of WTD treatment as described [9]. Briefly mice were fasted overnight (12—16h), and injected i.p.

 © 2025 The Author(s). Published by Elsevier GmbH. This is an open access article under the CC BY-NC-ND license (http://creativecommons.org/licenses/by-nc-nd/4.0/).

with glucose (1 g/kg body weight). Glycemia was measured at 0, 20′, 40′, 60′ and 120' minutes.

2.7. Transmission Electron Microscopy (TEM) analysis

For each mouse one fragment of the hepatic lobe was collected. Samples were fixed in 5% glutaraldehyde (Acros Organics, Thermo Fisher Scientific, Waltham, MA, USA) diluted in Sorensen phosphate buffer (0.1 M; pH 7.4) overnight at 4 °C, post-fixed with 1% osmium tetroxide in 0.1 M Sorensen phosphate buffer for 30 min, dehydrated, and araldite embedded (Fluka—Sigma Aldrich). Ultrathin sections were obtained with an Ultracut ultramicrotome (Reichert-Jung, Leica, Microsystems GmbH, Wetzlar, Germany), stained with uranyl acetate and lead citrate, and observed with Talos 120 (Thermo Fisher Scientific). Lipid droplets were quantified by ImageJ analysis of at least 10 photomicrographs per mouse. TEM images were acquired at 4300X magnification in randomly selected fields and the diameter (μm) of all lipid droplets present was measured. Results are expressed as average area (μm^2) and number of lipid droplet per area for each analyzed section. For representative images of mitochondria, a 11000X magnification was used.

2.8. Immunophenotyping of the blood and of cardiac Lymph Nodes (cLN)

Immunophenotyping was performed on 50 μl of fresh blood. Initially, the blood was incubated with a specific antibody mixture at room temperature for 30 min. Afterward, red blood cells were fixed and lysed using Fix& lyse 1x solution (Thermofisher), followed by two washes with PBS containing 2% FBS and 2 mM EDTA. Samples were then centrifuged at 1800 rpm for 5 min and cells were then used for staining. Cardiac lymph nodes (cLN) were weighted and then smashed on a 70 μm cell strainer with PBS containing 2% FBS and 2 mM EDTA. Cells were then stained for 30 min with superficial staining and washed with PBS containing 2% FBS and 2 mM EDTA. After centrifugation at 1800 rpm for 5 min the cells were resuspended in Fix and Perm buffer for 30 min at 4 °C (eBioscience Cat#00-5523-00). After the incubation the cells are treated with 3 times the volume of the fix and Perm with Perm buffer. After centrifugation the intracellular staining have been performed resuspending intracellular Ab with perm buffer. The following steps were performed according to manufacturer instruction. Samples were then acquired on a BD LSRFortessa™ X-20 cytometer and analyzed by Novoexpress software (version 1.6.0, Agilent, Santa Clara, CA, USA). The following antibody and (fluorophore) were used for blood staining [10]: antiCD45 (FITC), antiCD3 (AF700), antiCD11b (BUV737), antiLy6C (ef450), antiLy6G (BV650), antiCD27 (BB700), antiNK1 (APC) and antiCD11c (BV786). The following antibody and (fluorophore) were used for cLN staining: antiCD45 (FITC), antiCD3 (PerCpef710), antiCD4 (BUV737), antiCD8 (BUV805), antiCD44 (af700), antiCD62l (BV605), antiCD25 (BUV395), antiCD19 (PECY7), antiCD69 (APCef780), anti-FOXP3 (APC).

2.9. Proteomics sample preparation and analysis

Proteomics analysis was performed as previously described [11]. Briefly, protein were extracted from mice aorta (n = 6 LDLR and n = 6 $OPA1^{TG}$/LDLR KO on WTD) and mice liver (n = 3 LDLR and n = 3 $OPA1^{TG}$/LDLR KO on WTD) and analyzed using a Dionex Ultimate 3000 nano-LC system (Sunnyvale CA, USA) connected to an Orbitrap Fusion™ Tribrid™ Mass Spectrometer (Thermo Scientific, Bremen, Germany) equipped with a nano electrospray ion source operating in positive ion mode. Peptides identification was done using OpenMS software, a peptides identification approach combining the search engines as previously reported by our group, and a common contaminant proteins database (n = 179 proteins, https://github.com/pwilmart/fasta_utilities/blob/master/Thermo_contams.fasta). Data were processed and analyzed, as previously described [12—15]. Briefly, raw files were analyzed by the MaxQuant software (1) (version 2.5.0.0) and peak lists were searched against the Mouse Uniprot FASTA database (UP000000589.fasta, version October 2024). Cysteine carbamidomethylation was set as fixed modification, methionine oxidation and N-terminal protein acetylation as variable modifications. False discovery rate was 1% for proteins and peptides (minimum length of 7 amino acids) and was determined by searching a reverse database. Minimum peptides number was set to trypsin requiring C-terminal arginine or lysine with a maximum of two missed cleavages. LFQ minimum ratio count was set to 1 and Fast LFQ was deselected. Maximally allowed precursor mass deviation for peptide identification was 4.5 ppm after time dependent mass calibration and maximal fragment mass deviation was 20 ppm "Match between runs" was activated with a retention time alignment window of 20 min, and a match time window of 0.4 min. For total proteome analyses, solubility fractions were defined in MaxQuant for a combined protein MaxLFQ output, with a minimum ratio setting of 2. For fraction specific analyses no fraction information was predefined, and the minimum ratio setting was 1. All downstream bioinformatic analyses were performed with Perseus [15] (version 2.0.11). Data were log2-normalized and for the imputation of the missing values "Replace missing values from normal distribution" function was used with a width of 0.3 and a downshift of 1.8 over the total matrix. Student's t test was performed, corrected for the FDR. Gene Ontology (GO) and Kyoto Encyclopedia of Genes and Genomes (KEGG) enrichment analyses using the Database for Annotation, Visualization, and Integrated Discovery platform (DAVID; NIAID, Bethesda, MD) and Ingenuity Pathway Analysis (IPA; QIAGEN, Redwood City, CA) were performed as downstream analyses.

2.10. Liver/aorta histology and immunostaining

Slides were stained with Hematoxylin and Eosin (H&E) and Masson's Trichrome (Bio-Optica, Cat# 04—010802). Images were acquired with an optical microscope at a 5x (for the aorta), and 10X for the liver magnification using the AxioVision software. Immunofluorescence staining of aortic sections was performed using the antibody anti-Mac-2 (1:500; Cedarlane, Cat#CL8942AP) followed by anti-rat AF555 antibody (1:1000; Cat#A21434, Invitrogen) or anti-αSMA (1:200; Cat#NBP2-67440, Bio-Techne) followed by anti-rabbit AF555 antibody (1:1000; Cat# A27039, Invitrogen) and nuclei counterstaining with Hoechst (Sigma) respectively for assessing macrophage lesion infiltration and smooth muscle cells lesion content. Images were acquired with Zeiss confocal microscope at 4x or 5x magnification using the Zen software. Images were then analyzed with ImageJ software using a plug-in which considers the monochromatic components separately. Aortic root plaque area was calculated on Hematoxylin and Eosin (H&E)- stained sections. The percentage of collagen, Mac-2^+ and α-SMA^+ plaque areas were calculated as % of the plaque by dividing the positively stained plaque areas, of four sections, with the total plaque area.

2.11. Isolation and treatment of VSMCs

VSMCs were isolated from the aorta of LDLR and $OPA1^{TG}$/LDLR KO and cultured in DMEM high glucose medium with glutamine and antibiotics (Penicillin and Streptomycin) and 10% FBS as previously described by the laboratory [16]. VSMCs were used up to 10 passages. Before the experiments cells were treated overnight with 10%

 © 2025 The Author(s). Published by Elsevier GmbH. This is an open access article under the CC BY-NC-ND license (http://creativecommons.org/licenses/by-nc-nd/4.0/).

Lipoprotein Deficient Serum (LPDS) and then treated with mouse Platelet Derived Growth Factor bb (PDGFbb) at the concentration of 1 μM with LPDS. Gene expression analysis was performed by real time-PCR. RNA was extracted with Monarch total RNA miniprep kit (New England Biolabs) and cDNA was prepared by of 1 μg of total RNA, using the iScript cDNA Synthesis kit (Bio-Rad Laboratories). Amplification was carried out with LUNA® Universal qPCR Master Mix (New England BioLabs) in a CFX connect light cycler (BioRad, Cat#1708841). Expression was calculated using the ΔΔCt method and normalized to RPL13A as described [14,17].

2.12. Human atherosclerotic plaque samples

Clinical data and human carotid plaque tissue were obtained from the Carotid Plaque Imaging Project (CPIP; n = 78) [18]. The study protocol was approved by the Swedish ethical committee (472/2005, 2014/904, 60/2008, 2012/209). Written informed consent was provided by all participants.

In short, participants were included if they were eligible for carotid endarterectomy due to a stenosis degree >80% (measured by duplex ultrasound) without previous cerebrovascular symptoms (n = 27) or a stenosis degree >70% with cerebrovascular symptoms (ischemic stroke, transient ischemic attack, or amaurosis fugax; n = 51). Patients were followed post-operatively and information regarding future cardiovascular events was collected using the Swedish cause of death register and the Swedish National Inpatient Health Register.

All plaques were immediately frozen in liquid nitrogen. One cross-sectional fragment (1 mm) was taken from the most stenotic part of each plaque for RNA isolation. The isolated RNA isolated and sequenced using both Illumina HiSeq2000 and NextSeq 500 platforms, as previously described [19]. Briefly, transcript-level quantification was conducted using Salmon based on transcriptome release 27 of GENCODE in mapping-based mode. Gene counts were summarized using tximport and were normalized between samples using a trimmed mean of M-values (TMM) by edgeR [20], giving gene expressions as log2-transformed counts per million (CPM) after voom transformation. Batch effects of sequencing platforms were adjusted by an empirical Bayes method [21]. Differential gene expression analysis was performed to compare *OPA1* high (n = 39) and low (n = 39) groups (based on median *OPA1* plaque mRNA expression levels), as well as symptomatic (n = 51) and asymptomatic (n = 27) groups. Normalized Enrichment score (NES) was reported for enriched representative pathways from a gene set enrichment analysis [22]. P-values were adjusted using the Benjamini-Hochberg method. Kaplan–Meier survival analysis was used to examine if *OPA1* expression levels (in high and low groups) were associated with future postoperative cardiovascular events. P-value was reported from a log rank test.

2.13. Statistical analysis

Analyses were performed both on Microsoft Excel and Graph Pad-Prism, this latter also used for graphic presentation. Results are expressed as mean per group ± SEM and the statistical analyses between the two groups were performed by unpaired parametric two-sides T-test with a 95% confidence interval, when data sets tested normally distributed. Otherwise, Mann–Whitney nonparametric unpaired T-test were applied. A p-value of <0.05 was considered significant.

2.14. Data availability

The accession numbers for the proteomics data reported in this paper are available on ProteomeXchange repository with the following code: PXD060456 (Reviewer token: PwH7lGKwfTka), and PXD060450 (Reviewer token: SNm7LqXkZPCh).

The human data is protected due to privacy laws and would be shared upon request from a qualified academic investigator for the sole purpose of replicating the procedures and results presented in the article and providing that the data transfer is in agreement with European Union legislation on the general data protection regulation and decisions by the ethical review board of Sweden, the Region Skåne and the Lund University. Professor Isabel Goncalves (Isabel.Goncalves@med.lu.se) may be contacted for data access. Data regarding living subjects cannot be publicly available due to the sensitive nature of the data regulated by GDPR.

3. RESULTS

3.1. Optic Atrophy 1 (OPA1) overexpression results in increased plasma cholesterol levels in LDLR deficient mice

Eight weeks old OPA1^{TG}/LDLR KO mice and their controls (LDLR KO), were fed a cholesterol rich diet (WTD) for 12 weeks (Figure 1A). At sacrifice OPA1^{TG}/LDLR KO presented a significant increase in plasma cholesterol levels compared to LDLR KO (Figure 1B). A difference mainly related to increased cholesterol content in both very low-density lipoprotein (VLDL) and in low-density lipoprotein (LDL) particles (Figure 1C). Plasma triglycerides (TG) levels and their distribution in lipoprotein classes were similar between the experimental groups. (Figure 1D and E). We previously demonstrated that OPA1 deficiency impacts bile acids production [4], therefore we investigated whether this is true also when OPA1 is overexpressed. The analysis of the bile acids pool in the liver showed that, despite a similar amount of bile acids (Figure 1F), OPA1^{TG}/LDLR KO livers, presented a significant reduction in primary unconjugated bile acids such Murocolic Acid-beta (MCA β), and an increase in primary conjugated bile acids such as Glycocholic Acid (GCA) and Taurocholic Acid (TCA) (Figure 1G) compared to control mice. Accordingly, Taurochenodeoxycholic Acid (TCDCA) and Glycochenodeoxycholic Acid (GCDCA) were increased in the liver of OPA1^{TG}/LDLR KO mice (Sup. Figure 1A). Overall, a significant reduction in the percentage of primary unconjugated bile acids and a significant increase in conjugated bile acids were observed (Figure 1H). This finding suggests increased lipid absorption from dietary sources, a hypothesis further supported by the significantly elevation in plasma triglyceride (TG) levels observed in OPA1^{TG}/LDLR KO mice compared to LDLR KO mice during the oral lipid tolerance test (Figure 1I). Moreover, hepatic levels of free secondary bile acids were significantly reduced (Sup. Figure 1B), indicating a potential protective role of OPA1 overexpression in the detoxification of hydrophobic bile acids. Notably, this effect occurred without significant changes in the expression of hepatic bile acid transporters ATP-Binding cassette G5 (ABCG5), ATP-Binding cassette G8 (ABCG8), or the Farnesoid X receptor (FXR) (Sup. Figure 1C).

Notably, weight gain was similar in the two experimental groups (Sup Figure 1D) and the same was true for the weight of liver, pancreas, heart, Visceral Adipose Tissue (VAT), Subcutaneous Adipose Tissue (SCAT) and Brown Adipose Tissue (BAT) at sacrifice (Sup. Figure 1E). Also, key markers of liver and kidney function such as Alanine Aminotransferase (ALT), Aspartate Transferase (AST) (Sup. Figure 1F), Creatinine, Blood Urea Nitrogen (BUN) (Sup. Figure 1G) were not different between the experimental models suggesting that there is no liver damage when OPA1 is overexpressed.

Moreover, the absence of major changes in glucose tolerance (Sup. Figure 1H) suggest that OPA1 overexpression result in a metabolic phenotype that is peculiar for lipoprotein metabolism.

 © 2025 The Author(s). Published by Elsevier GmbH. This is an open access article under the CC BY-NC-ND license (http://creativecommons.org/licenses/by-nc-nd/4.0/).

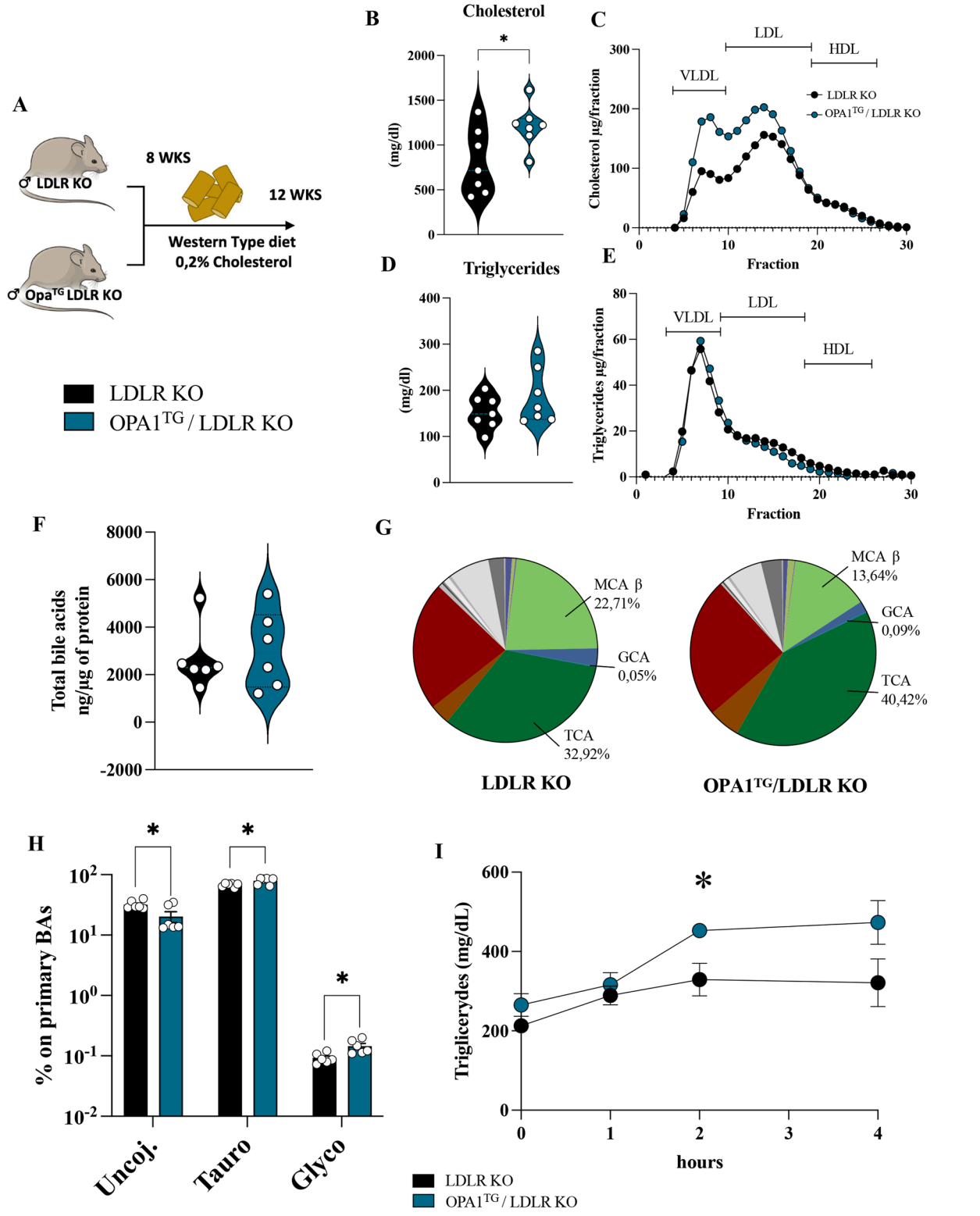

Figure 1: Systemic overexpression of Opa1 results in increased plasma cholesterol levels due to changes in bile acids release and fat solubilization.
(A) Summary of the experimental approach. (B) Plasma cholesterol levels and (C) Cholesterol distribution in lipoprotein fractions. (D) Plasma triglycerides levels and (E) triglycerides distribution in lipoprotein fractions (Data are shown as means ± SEM; n = 7 for each experimental group) (*p < 0.05, by Student's t test) (F) Bile acid content in the liver. (G) Relative distribution of bile acids within the total bile pool in the liver; key significant components affected are highlighted. (H) Distribution of unconjugated (Uncoj.), taurine conjugated, and glycol conjugated bile acids among primary bile acids in the liver (BAs) (Data are shown as means ± SEM; n = 6 for each experimental group) (*p < 0.05 by One Way Anova). (I) Changes in plasma triglyceride levels following an Oral Lipid Tolerance Test (OLTT) (Data are shown as means ± SEM; n = 5 for LDLR and n = 5 for OPA1^{TG}/LDLR KO). (*p < 0.05, by One Way Anova).

 © 2025 The Author(s). Published by Elsevier GmbH. This is an open access article under the CC BY-NC-ND license (http://creativecommons.org/licenses/by-nc-nd/4.0/).

3.2. OPA1 overexpression alters lipid and lipoproteins-related proteome in the liver

To understand whether the changes observed in lipid metabolism in OPA1^{TG} mice could be the result of altered liver lipid metabolism, we performed untargeted liver proteomic analysis and observed several changes in the proteome of OPA1^{TG}/LDLR KO compared to LDLR KO (Figure 2A). As expected, most of the differently expressed proteins were those related to mitochondrial function and ATP synthesis (Figure 2B), a finding concordant with the presence of smaller (Sup. Figure 1I) and rounder (Sup. Figure 1J) mitochondria observed in OPA1^{TG}/LDLR KO, which were also more electron-dense (Figure 2C). The overactivation of hepatocyte mitochondrial fusion coupled to the findings from proteomics would suggest an increased metabolic activity in the hepatocytes. Indeed, the specific analysis of proteins related to lipid metabolism, revealed that most of the genes involved in bile acid synthesis and conjugation including aldo-keto reductase 1D1 (AKR1D1), Alpha-Methylacyl-CoA Racemase (AMACR), Bile Acid-CoA:Amino Acid N-Acyltransferase (BACS) and Cyp27a1 (Figure 2D) as well as those involved in lipoprotein production such as apolipoprotein (Apo) like Apoa1, Apoa2, Apoa4, Apoa5, ApoB, Apoc1, Apoc2, Apoc3 and ApoE (Figure 2E) were significantly upregulated in OPA1^{TG}/LDLR KO compared to LDLR KO animals. At the histological level, changes in liver lipid metabolism were reflected by increased ectopic fat deposition in OPA1^{TG}/LDLR KO mice compared to LDLR KO mice (Figure 2F,G), while no changes in fibrosis were observed (Figure 2H, I).

3.3. Systemic OPA1 overexpression results in a more fibrotic atherosclerotic plaque

Next, we investigated whether the impact of OPA1 overexpression on lipid metabolism might affect atherosclerotic plaque formation. OPA1^{TG}/LDLR KO mice displayed a significant increase in atherosclerotic plaque area through-out the aorta (Figure 3A,B). Interestingly, the atherosclerotic plaques in OPA1^{TG}/LDLR KO mice were more fibrotic compared to those from LDLR KO (Figure 3 C) while VMCSs distribution in the atherosclerotic plaque was similar in OPA1^{TG}/LDLR KO plaque compared to LDLR KO (Figure 3D,E). Mac2 positive macrophage were less in OPA1^{TG}/LDLR KO (Figure 3E,F) while a similar distribution of lymphocytes subsets was detected in the lymph nodes draining the aorta, thus excluding differences in the activation of systemic immune response (Sup. Figure 2A). A hypothesis further supported by the finding of similar profiles of circulating leukocytes (CD45+), including monocytes, neutrophils, NK cells, B and T lymphocytes between experimental groups (Sup. Figure 2B).

3.4. Hepatic OPA1 deficiency protects from atherosclerosis

In line with these findings, when we investigated the impact of hepatocyte deletion of OPA1 on the circulating lipid profile, by comparing the OPA1$^{\Delta Hep}$/LDLR KO fed with WTD and controls, we observed a significant reduction in plasma cholesterol levels (Figure 4A) and plasma TG levels (Figure 4B) together with a reduction of both cholesterol (Figure 4C) and triglycerides (Figure 4D) on both VLDL and LDL. Accordingly, the development of the atherosclerotic lesion was reduced in OPA1$^{\Delta Hep}$/LDLR KO mice (Figure 4E,F). Interestingly OPA1 hepatocyte selective deficiency did not affect plaque composition and VSMCs distribution (Figure 4E,G). This prompted us to investigate plaque changes and VMSCs signature in OPA1^{TG}/LDLR KO mice.

3.5. Systemic OPA1 overexpression affects plaque composition

To clarify changes in atherosclerotic plaque characteristics, untargeted proteomic analysis was performed in the aorta from OPA1^{TG}/LDLR KO and LDLR KO controls. A total of 942 proteins were quantified, and out of these proteins n = 161 were significantly affected (p-value <0,05). 13 proteins were upregulated (log2FC > 1) and 26 were downregulated (log2FC < −1; Figure 5A, B). Ingenuity Pathway Analysis (IPA) revealed that metabolic pathways, including glycolysis, glucose metabolism, the Electron Transport Chain (ETC), and the Tricarboxylic Acid (TCA) cycle, were upregulated, indicating an increased oxidative metabolism in OPA1^{TG}/LDLR KO mice (Figure 5C). In contrast, pathways related to cell migration, survival, differentiation, and extracellular matrix degradation were downregulated compared to controls (Figure 5C). Consistently, upstream regulator analysis showed a significant inhibition (z-scores < −2) for key modulators of plaque phenotype, such as Transforming Growth Factor beta 1 (TGFB1) and Krüppel-Like Factor 4 (KLF4), potentially explaining the observed reduction in macrophage plaque content which coupled with a decreased expression of Matrix Metalloprotease 9 (MMP9). Conversely, the upregulated upstream regulators are those involved in metabolic processes as Peroxisome Proliferator-Activated Receptor alpha (PPAR α), Mammalian Target Of Rapamycin (MTOR) and Hepatocyte Nuclear Factor-4alpha (HNF4 α) (Figure 5D). Taken together, these data suggest that overexpression of OPA1, by leading to an increased oxidative metabolism might affect Vascular Smooth Muscle Cells (VSMCs) predisposition to migrate and differentiate (Figure 5E and Sup. Figure 3). Further analysis on downregulated, differentially expressed proteins, shows a significant enrichment in those pathways involved in supramolecular complexes, fiber, cytoskeleton (Figure 5F). These changes prompted us to isolate VSMCs from the aorta and test them in the presence of Lipoprotein Deficient Serum (LPDS) 10%, plus/minus Platelet Derived Grow Factor bb (PDGFbb) (1 μM) (Figure 5G). αSMA expression was significantly higher in OPA1^{TG}/LDLR KO cells compared to controls at baseline and decreased following incubation with PDGFbb (Figure 5H). This was not paralleled by an increase in markers indicating a switch toward a synthetic phenotype foam cell (CD68; Figure 5H) or fibroblast transition (KLF4; Figure 5H). The expression of MMP9 and Matrix Metalloprotease 2 (MMP2; Figure 5H) which are involved in extracellular matrix remodeling in the plaque, were significantly downregulated in OPA1^{TG}/LDLR KO compared to LDLR KO controls, confirming potential changes in plaque composition highlighted by proteomic analysis.

3.6. Increased OPA1 expression in human plaque is associated with changes in genes involved in plaque morphology

To translate these findings into the human context we explored differences in the transcriptome of carotid plaques of asymptomatic and symptomatic patients. Plaque *OPA1* mRNA levels were not significantly associated with symptoms at base line or cardiovascular events during follow-up (Figure 6A,B). Upregulated genes in the *OPA1* high plaques were enriched in *MTORC1*, lipid catabolism, cell replication, DNA repair and cell activation pathways (Figure 6C), these findings suggest a transcriptional program favoring mitochondrial activity, metabolic efficiency, and proliferative readiness; whereas upregulated genes in the *OPA1* low plaques were enriched in cell growth, tissue migration, cellular differentiation and smooth muscle cell associated pathways (Figure 6C). In line with mouse data and in vitro experiments, TGF beta signaling pathway is downregulated, suggesting that elevated OPA1 expression limits VSMCs metabolic switch as supported also by increased MTORC1 activation. Elevated OPA1 expression is also associated with improved lipid trafficking and catabolism further supporting

 © 2025 The Author(s). Published by Elsevier GmbH. This is an open access article under the CC BY-NC-ND license (http://creativecommons.org/licenses/by-nc-nd/4.0/).

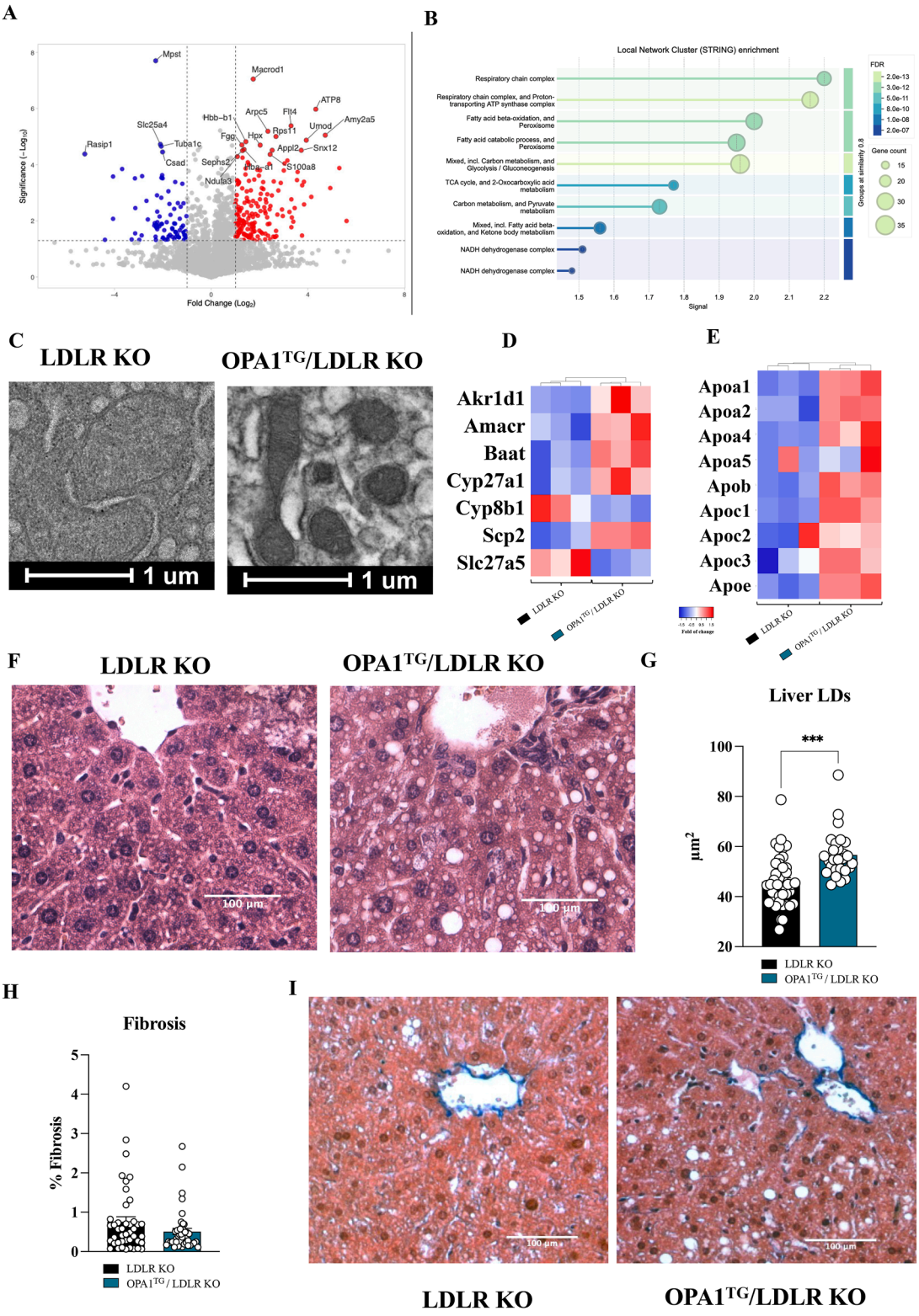

Figure 2: The overexpression of Opa1 results in increased hepatic lipid accumulation and mitochondrial dysfunction.
(A) Volcano plot from untargeted liver proteomics. (B) String Local Network Cluster for liver proteomics data from LDLR and OPA1^{TG}/LDLR KO mice. (C) Representative image of transmission electron microscopy of mitochondria from LDLR and OPA1^{TG}/LDLR KO mice. (D) Changes in the expression of proteins involved in bile acids synthesis (Data are shown as fold of change; n = 3 for each experimental group). (E) Changes in the expression of proteins involved in lipoprotein synthesis (Data are shown as fold of change; n = 3 for each experimental group). (F) Representative images of liver sections stained with hematoxylin and eosin from LDLR and OPA1^{TG}/LDLR KO mice (scale bar 100 µm). (G) Average area of liver Lipid droplets (LDs) in LDLR KO (black bar) and OPA1^{TG}/LDLR KO (green bar) mice. (H) Percentage of hepatic fibrosis from the quantification of liver section stained with Masson's trichrome (I). (Data are shown as fold of change; n = 5 for each experimental group). (*$p < 0.05$, and **<0.001 by Student's t test or One Way Anova for multiple comparison).

 © 2025 The Author(s). Published by Elsevier GmbH. This is an open access article under the CC BY-NC-ND license (http://creativecommons.org/licenses/by-nc-nd/4.0/).

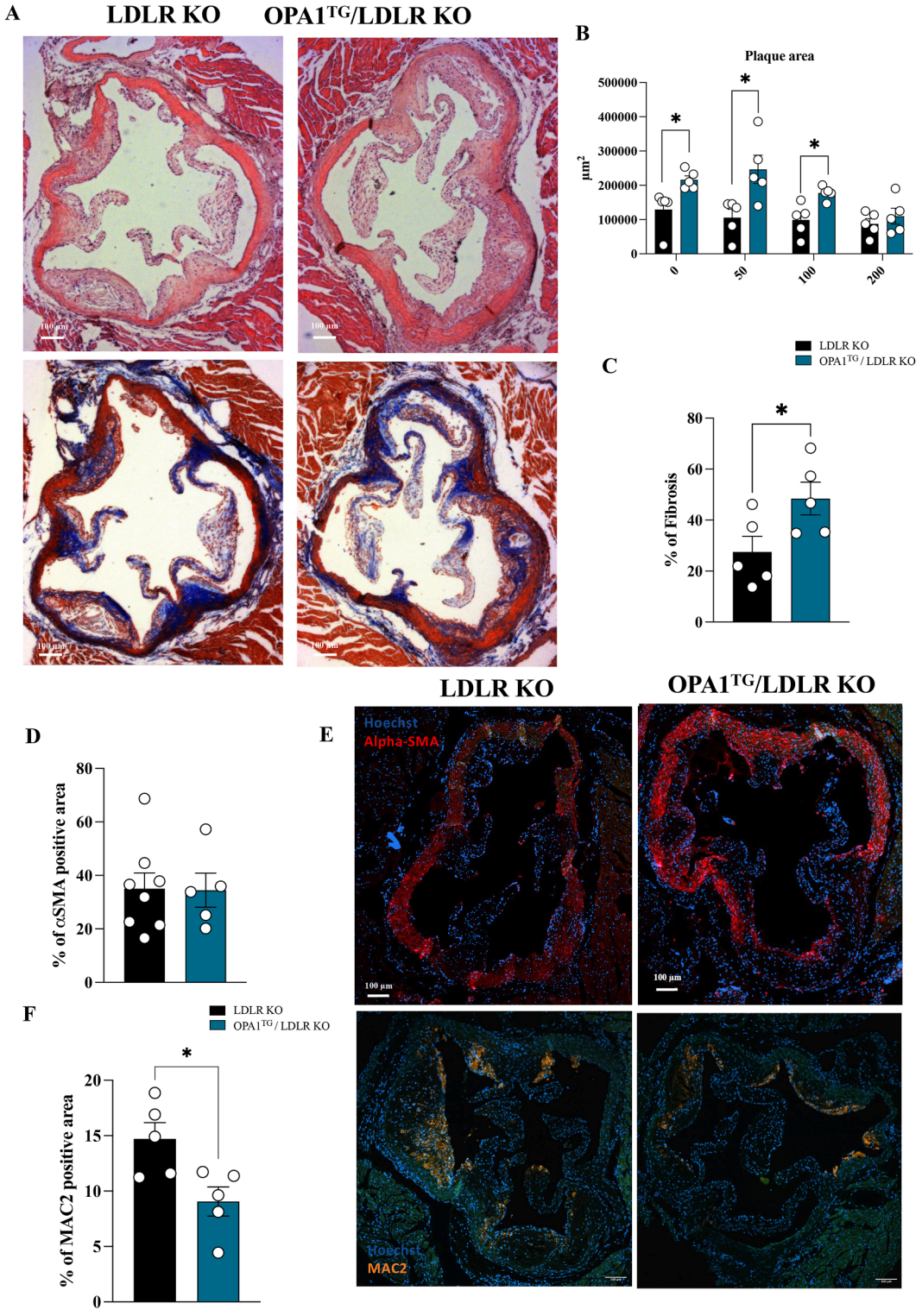

Figure 3: OPA1 overexpression of results in increased atherosclerosis, coupled to fibrosis, but a similar distribution of VSMCs and macrophages in the atherosclerotic lesion.

(A) Representative image of the aorta from LDLR and OPA1^{TG}/LDLR KO mice stained with hematoxylin and eosin and Masson's trichrome (scale bar 100 µm). (B) Atherosclerotic plaque area at the aortic root (0 µM) an at 50, 100 and 200 µm from the sinus. (Data are shown as means ± SEM; n = 5 for each experimental group). (C) Percentage of fibrosis in the aorta following Masson's trichrome staining. (Data are shown as means ± SEM; n = 5 for each experimental group). (D) Percentage of alpha actin (αSMA) positive area within the atherosclerotic plaque area (Data are shown as means ± SEM; n = 8 for LDLR and n = 5 for OPA1^{TG}/LDLR KO). (E) Representative images for αSMA and MAC2 staining in the aorta form LDLR and OPA1^{TG}/LDLR KO (scale bar 100 µm). (F) MAC2 (galectin-3) positive area within the atherosclerotic plaque area (Data are shown as means ± SEM; n = 6 for LDLR and n = 5 for OPA1^{TG}/LDLR KO) (*$p < 0.05$, by Student's t test).

 © 2025 The Author(s). Published by Elsevier GmbH. This is an open access article under the CC BY-NC-ND license (http://creativecommons.org/licenses/by-nc-nd/4.0/).

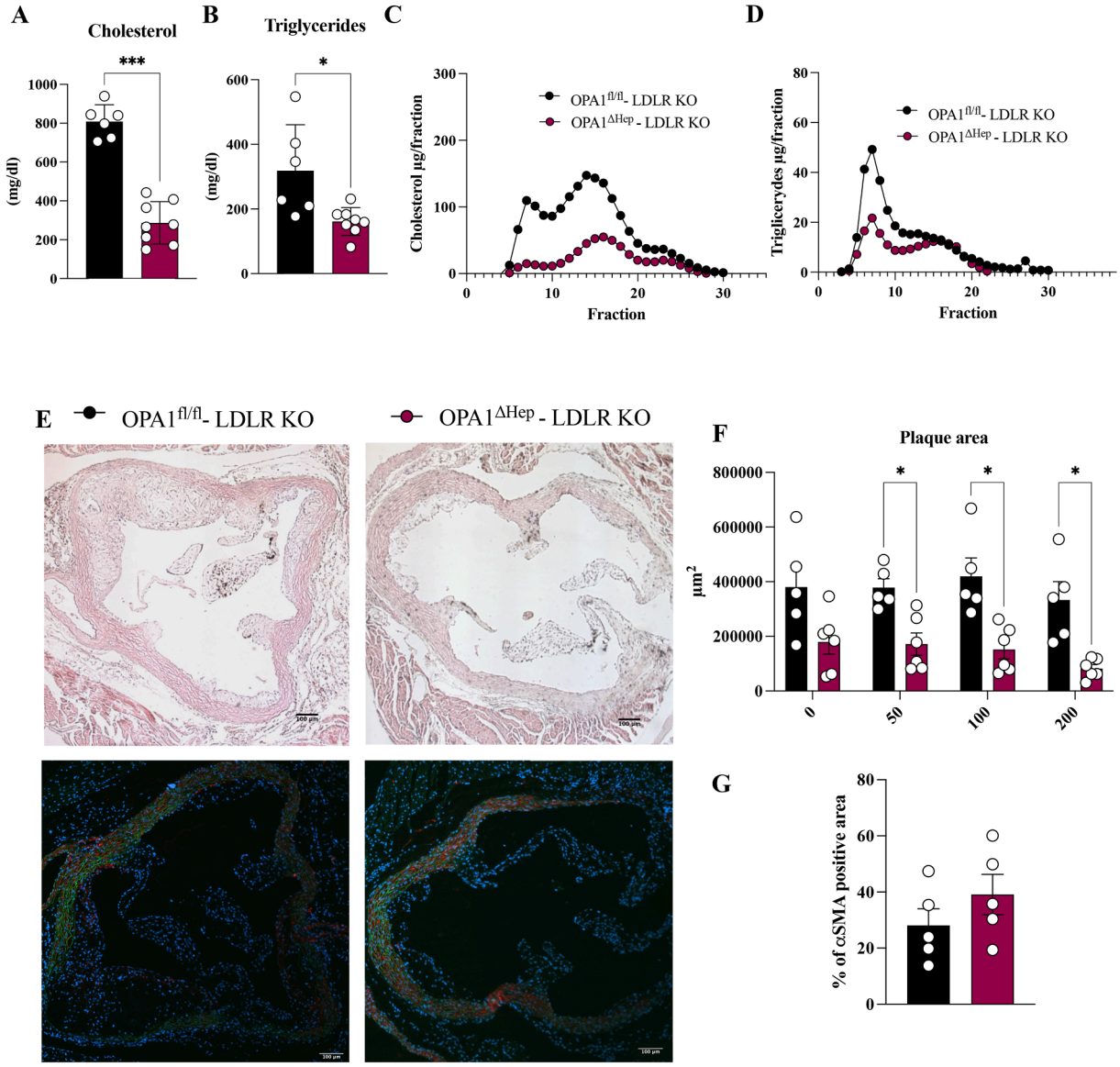

Figure 4: OPA1 hepatocyte deficiency significantly affects the systemic levels of cholesterol and the development of the atherosclerotic lesion.
Plasma (A) Cholesterol and (B) Triglyceride levels in OPA1$^{\Delta Hep}$/LDLR KO and OPA1$^{fl/fl}$/LDLR KO are presented. (C) Cholesterol and (D) Triglycerides distribution in lipoprotein fractions. (E) Representative images from hematoxylin and eosin and αSMA staining of the aorta of OPA1$^{\Delta Hep}$/LDLR KO and OPA1$^{fl/fl}$ -LDLR KO mice (scale bar 100 µm). (F) Changes in plaque area in the aortic root (0 µM) and at 50, 100 and 200 µm from the aortic sinus. (Data are shown as means ± SEM). (G) Percentage of alpha actin (αSMA) positive area within the plaque area of OPA1$^{\Delta Hep}$/LDLR KO and OPA1$^{fl/fl}$/LDLR KO mice. (*$p < 0.05$, and ***<0.001 by Student's t test or One Way Anova for multiple comparison).

the role of OPA1 in preventing the development of synthetic phenotype in VSMCs.

4. DISCUSSION

We have previously shown that hepatocyte-specific OPA1 deletion impairs lipid absorption by disrupting organelle tethering and sterol trafficking [4]; in this study, we demonstrate that systemic OPA1 overexpression profoundly affects hepatic lipoprotein metabolism, resulting in increased plasma cholesterol levels and enhanced atherogenesis.

More in details, we show, in an atherogenic context, that OPA1 plays a dual role: i) modulates hepatic lipid handling and ii) directly impacts vascular smooth muscle cells (VSMCs) biology. In LDLR knockout (LDLR KO) mice, OPA1 overexpression is associated with increased lipid droplet accumulation and elevated levels of primary and secondary conjugated bile acids in the liver, suggesting enhanced dietary lipid absorption. Conversely, a reduction in secondary unconjugated bile acids suggests a protective effect through decreased accumulation of cytotoxic, insoluble bile acids. Of note, while OPA1 overexpression leads to hypercholesterolemia and increased atherosclerosis, VSMC within the plaques of OPA1^{TG}/LDLR KO mice are less synthetic compared to those of LDLR KO mice.

To further investigate the direct impact of OPA1 on VSMC cellular metabolism, VSMCs were isolated from the aortas of OPA1^{TG}/LDLR KO and LDLR KO mice and stimulated with PDGF-BB. VSMCs from

 © 2025 The Author(s). Published by Elsevier GmbH. This is an open access article under the CC BY-NC-ND license (http://creativecommons.org/licenses/by-nc-nd/4.0/).

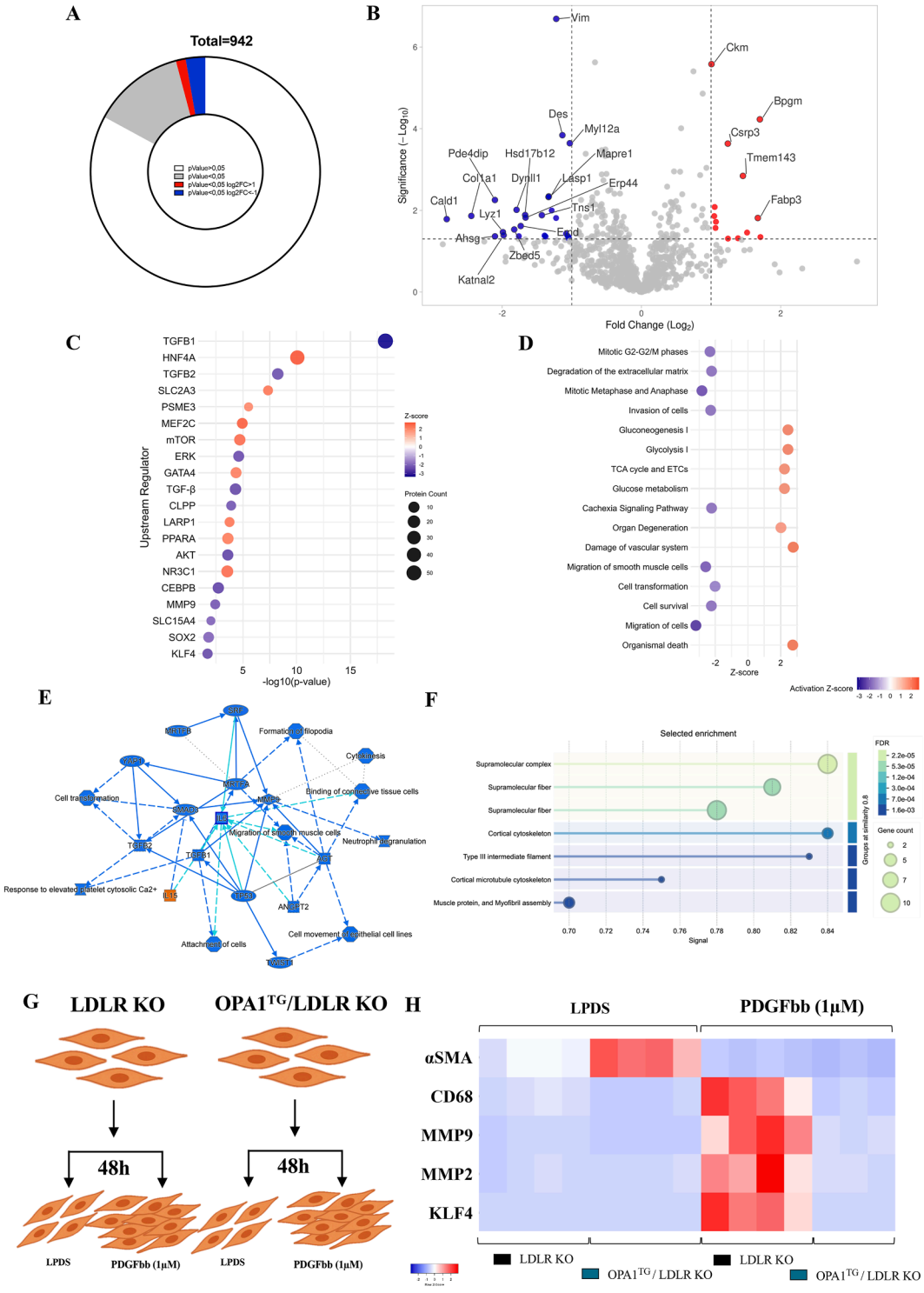

Figure 5: OPA1^{TG}/LDLR KO mice present and increased cell metabolic activity within the atherosclerotic plaque.
(A) Untargeted proteomic was performed on mouse aorta protein extract from 6 LDLR and 6 OPA1^{TG}/LDLR KO mice and identified 942 proteins in both samples. (B) The top differentially expressed proteins from aorta proteomics and (C) changes in key metabolic processes, tissue adaptation, and cells cycle pathways are reported. (D) Analysis of upstream regulators down and upregulated in OPA1^{TG}/LDLR KO compared to LDLR KO mice. (E) Interconnection of the pathways affected in OPA1^{TG}/LDLR KO compared to LDLR KO mice; downregulated pathways are represented in blue, while upregulated pathways in Orange. (F) String Local Network Cluster on downregulated Differentially expressed proteins from proteomics data of LDLR and OPA1^{TG}/LDLR KO aorta. (*$p < 0.05$, and ***<0.001 by Student's t test or One Way Anova for multiple comparison). (G) VSMCs were isolated from OPA1^{TG}/LDLR KO and LDLR KO aorta were treated 48h with LPDS (lipoprotein deficient serum) with or without PDGFbb (1 μM) (Platelets Derived Growth Factor BB). (H) Alpha Actin (aSMA), Cluster of Differentiation 68 (CD68), Matrix MetalloProteinase-9 (MMP-9), Matrix MetalloProteinase-2 (MMP-2) and Krüppel-Like Factor 4 (KLF4) expression is shown as a fold of change against LDLR KO VSMCs treated with LPDS normalized on Ribosomal Protein Ligand 13a (RPL13a). (Data are shown as means ± SEM).

 © 2025 The Author(s). Published by Elsevier GmbH. This is an open access article under the CC BY-NC-ND license (http://creativecommons.org/licenses/by-nc-nd/4.0/).

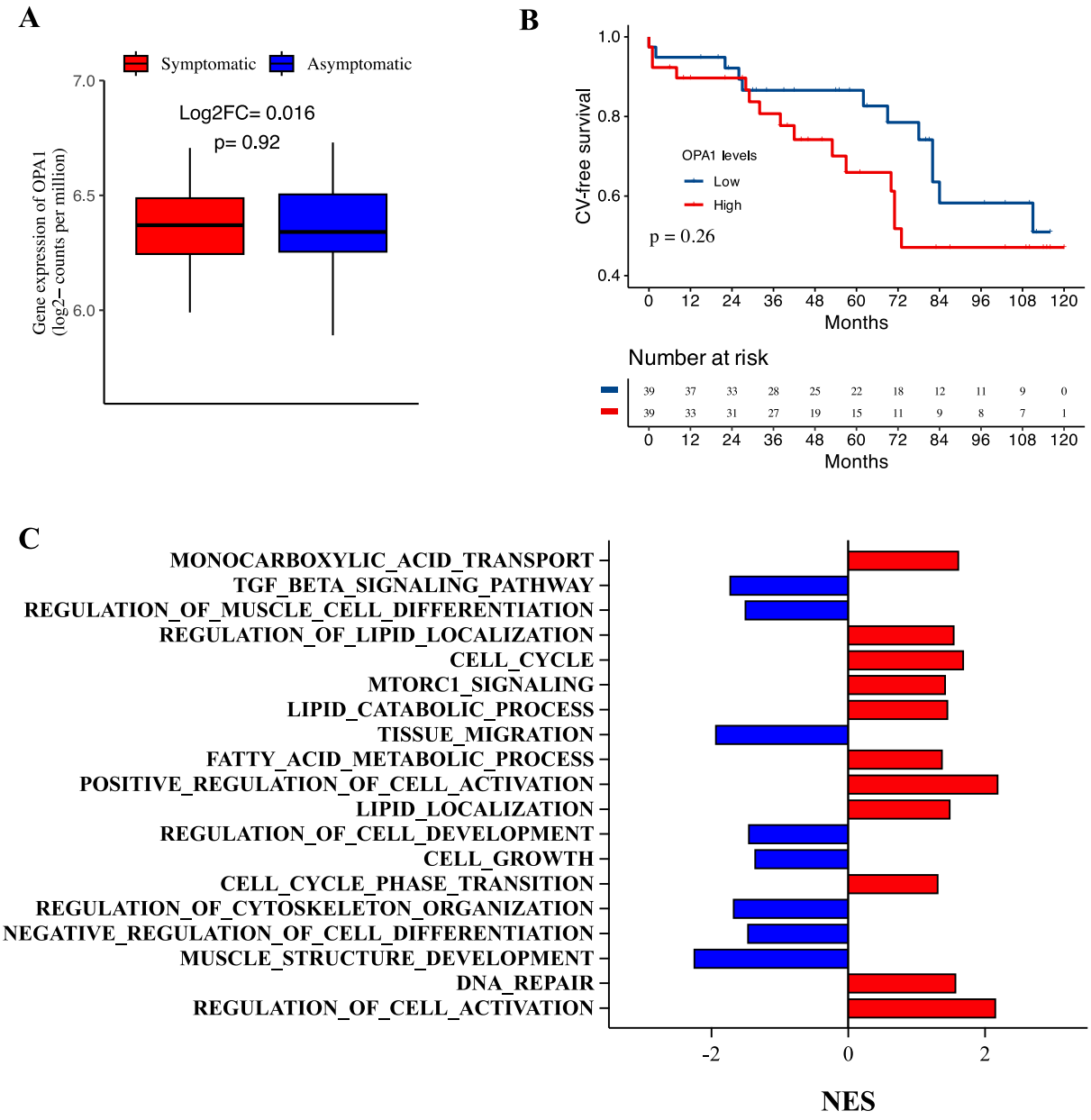

Figure 6: Association of OPA1 expression in human carotid plaques with plaque features.
(A) Human carotid plaque mRNA levels of *OPA1,* did not differ between symptomatic (n = 57) and asymptomatic plaques (n = 21). (B) Kaplan Meier curve showing that higher plaque mRNA levels of OPA*1* (above median) were not significantly associated with an increased risk of future cardiovascular events (n = 39 in both groups). (C) Normalized Enrichment Score (NES) of the enriched pathways from a gene set enrichment analysis, comparing gene expressions between high (n = 39) and low (n = 39) *OPA1* group in human carotid plaques. (*p < 0.05, and ***<0.001).

OPA1^{TG}/LDLR KO mice displayed reduced proliferation and decreased expression of matrix metalloproteinases, indicating a more quiescent and less degradative phenotype compared to the counterpart isolated from LDLR KO mice.

These findings were further supported by analyses of human carotid artery specimens. Samples exhibiting higher OPA1 expression OPA1 expression are not directly associated with differences in the prevalence of clinical symptoms or cardiovascular outcome, yet it defines distinct molecular signatures that provide novel insights into plaque biology. Higher OPA1 expression was associated with the upregulation of mTORC1 signalling, lipid catabolism, DNA repair, and cell activation pathways—all hallmarks of metabolically active vascular cells. These transcriptional features are consistent with a preserved mitochondrial network coupled to a contractile VSMC phenotype via enhanced mitochondrial dynamics and energy metabolism. Notably, the downregulation of TGF-β signalling in carotid plaques with higher OPA1 expression is in line with previous in vitro and in vivo data indicating that TGF-β preserves VSMC quiescence and inhibit phenotypic switching. Together, these findings indicate that in human carotid plaques OPA1 expression reflects metabolic configuration within the plaque microenvironment. These observations strengthen the relevance of mitochondrial dynamics in vascular cell fate and plaque physiopathology, offering a mechanistic bridge between metabolic signalling and structural integrity in

 © 2025 The Author(s). Published by Elsevier GmbH. This is an open access article under the CC BY-NC-ND license (http://creativecommons.org/licenses/by-nc-nd/4.0/).

human atherosclerosis. Moreover, these findings suggest to evaluate the relevance of OPA1 on the evolution of atherosclerosis in other vascular districts, where the impact of hemodynamic and rheological factors is less relevant.
In conclusion, our findings reveal a complex role of OPA1 in atherosclerosis, acting as both a systemic metabolic modulator and within the vasculature. Future studies should explore therapeutic strategies aimed at modulating mitochondrial plasticity in the liver, which may offer a novel means to control lipoprotein metabolism and reduce cardiovascular risk.

ACKNOWLEDGMENTS

The authors would like to thank the core facilities from Università degli Studi di Milano, OMICS for LC-MS/MS analysis and NOLIMITS, the advanced imaging facility. Figures were created using pictures from Servier Medical Art, by Servier (http://smart.servier.com).

CRediT AUTHORSHIP CONTRIBUTION STATEMENT

Lorenzo Da Dalt: Writing — original draft, Supervision, Project administration, Methodology, Investigation, Funding acquisition, Formal analysis, Data curation, Conceptualization. **Francesca Fantini:** Methodology, Data curation. **Giulia Giancane:** Methodology, Investigation, Formal analysis, Data curation. **Annalisa Moregola:** Methodology. **Silvia Roda:** Methodology, Formal analysis. **Monika Svecla:** Methodology, Formal analysis. **Silvia Pedretti:** Methodology, Formal analysis, Data curation. **Giovanni Battista Vingiani:** Methodology, Data curation. **Jiangming Sun:** Methodology, Data curation. **Andreas Edsfeldt:** Writing — original draft, Visualization, Supervision. **Isabel Goncalves:** Writing — original draft, Visualization, Validation. **Patrizia Uboldi:** Methodology. **Elena Donetti:** Methodology, Investigation. **Andrea Baragetti:** Visualization, Validation, Supervision, Methodology, Funding acquisition. **Nico Mitro:** Writing — original draft, Visualization, Validation. **Luca Scorrano:** Writing — original draft, Visualization, Validation. **Giuseppe Danilo Norata:** Writing — original draft, Project administration, Investigation, Funding acquisition, Conceptualization.

DECLARATION OF COMPETING INTEREST

A.E. reports consulting fees from Novo Nordisk, Sanofi and Amgen, but this has not had any relationship with the current study or affected the design/outcome of the study. G.D.N. reports speaker bureau and consulting fees from Amgen, Daichii, Meda Pharma, Menarini, MSD, Novartis and Sanofi which are unrelated to this manuscript. All the other authors do not report any conflict of interest.

FUNDINGS

The results of this research project have been founded by the European Atherosclerosis Society (EAS) Research grant 2023 to Lorenzo Da Dalt. Part of this project have also been founded by Progetti di Rilevante Interesse Nazionale (PRIN 2022 7KTSAT to GDN); Progetti di Rilevante Interesse Nazionale (PRIN-PNRR 2022 P202294PHK to A. B.); PNRR Missione 4 (Progetto CN3 - National Center for Gene Therapy and Drugs based on RNA Technology to GDN); PNRR Missione 4 (Progetto MUSA- Multilayered Urban Sustainability Action to GDN); PNRR Missione 6 (PNRR-MAD-2022-12375913 to GDN); CARDINNOV, Ministry of Research and University under the umbrella of the Partnership Fostering a European Research Area for Health (ERA4Health) (GA N° 101095426 of the EU Horizon Europe Research and Innovation Programme to GDN). The work including the CPIP biobank was supported by the Swedish Society for Medical Research [A.E., CG-22-0254-H-02], the Swedish Research Council [I.G. 2019-01260 and 2023—02368; AE. 2019-01907 and 2024—02761; J.S. 20241210] The Swedish Heart and Lung Foundation [A.E.20220044 and 20220284; I.G., 20200403 and 20230257], the Swedish Stroke Association [J.S., S-993166], Skåne University hospital [A.E.; I.G.] and Lund University Diabetes Center (Swedish Research Council—Strategic Research Area Exodiab Dnr 2009-1039 and the Swedish Foundation for Strategic Research Dnr IRC15-0067), the LeDucq Foundation Network of Excellence: CHECKPOINT ATHERO [22CVD02 to IG], the Knut and Alice Wallenberg foundation, the Medical Faculty at Lund University and Region Skåne [N/A to AE]. Silvia Pedretti is supported by Fondazione Umberto Veronesi post-doctoral fellowship.

DATA AVAILABILITY

Data will be made available on request.

APPENDIX A. SUPPLEMENTARY DATA

Supplementary data to this article can be found online at https://doi.org/10.1016/j.molmet.2025.102256.

REFERENCES

[1] Pirillo A, Casula M, Olmastroni E, Norata GD, Catapano AL. Global epidemiology of dyslipidaemias. Nat Rev Cardiol 2021;18:689—700. https://doi.org/10.1038/s41569-021-00541-4.
[2] Madamanchi NR, Runge MS. Mitochondrial dysfunction in atherosclerosis. Circ Res 2007;100:460—73. https://doi.org/10.1161/01.RES.0000258450.44413.96.
[3] Osellame LD, Blacker TS, Duchen MR. Cellular and molecular mechanisms of mitochondrial function. Best Pract Res Clin Endocrinol Metabol 2012;26:711—23. https://doi.org/10.1016/j.beem.2012.05.003.
[4] Da Dalt L, Moregola A, Svecla M, Pedretti S, Fantini F, Ronzio M, et al. The inhibition of inner mitochondrial fusion in hepatocytes reduces non-alcoholic fatty liver and improves metabolic profile during obesity by modulating bile acid conjugation. Cardiovasc Res 2024;119:2917—29. https://doi.org/10.1093/cvr/cvad169.
[5] Bonacina F, Da Dalt L, Catapano AL, Norata GD. Metabolic adaptations of cells at the vascular-immune interface during atherosclerosis. Mol Aspect Med 2021;77:100918. https://doi.org/10.1016/j.mam.2020.100918.
[6] Li J, Li X, Song S, Sun Z, Li Y, Yang L, et al. Mitochondria spatially and temporally modulate VSMC phenotypes via interacting with cytoskeleton in cardiovascular diseases. Redox Biol 2023;64:102778. https://doi.org/10.1016/j.redox.2023.102778.
[7] Docherty CK, Carswell A, Friel E, Mercer JR. Impaired mitochondrial respiration in human carotid plaque atherosclerosis: a potential role for Pink1 in vascular smooth muscle cell energetics. Atherosclerosis 2018;268:1—11. https://doi.org/10.1016/j.atherosclerosis.2017.11.009.
[8] Xia Y, Zhang X, An P, Luo J, Luo Y. Mitochondrial homeostasis in VSMCs as a central hub in vascular remodeling. Int J Mol Sci 2023;24. https://doi.org/10.3390/ijms24043483.
[9] Da Dalt L, Ruscica M, Bonacina F, Balzarotti G, Dhyani A, Di Cairano E, et al. PCSK9 deficiency reduces insulin secretion and promotes glucose intolerance: the role of the low-density lipoprotein receptor. Eur Heart J 2019;40:357—68. https://doi.org/10.1093/eurheartj/ehy357.
[10] Svecla M, Moregola A, Dalt L Da, Nour J, Baragetti A, Uboldi P, et al. ASGR1 deficiency improves atherosclerosis but alters liver metabolism in ApoE-/-

 © 2025 The Author(s). Published by Elsevier GmbH. This is an open access article under the CC BY-NC-ND license (http://creativecommons.org/licenses/by-nc-nd/4.0/).

mice. Cardiovasc Diabetol 2024;23:428. https://doi.org/10.1186/s12933-024-02507-5.

[11] Da Dalt L, Castiglioni L, Baragetti A, Audano M, Svecla M, Bonacina F, et al. PCSK9 deficiency rewires heart metabolism and drives heart failure with preserved ejection fraction. Eur Heart J 2021;42:3078–90. https://doi.org/10.1093/eurheartj/ehab431.

[12] Cox J, Mann M. MaxQuant enables high peptide identification rates, individualized p.p.b.-range mass accuracies and proteome-wide protein quantification. Nat Biotechnol 2008;26:1367–72. https://doi.org/10.1038/nbt.1511.

[13] Tyanova S, Temu T, Sinitcyn P, Carlson A, Hein MY, Geiger T, et al. The perseus computational platform for comprehensive analysis of (prote)omics data. Nat Methods 2016;13:731–40. https://doi.org/10.1038/nmeth.3901.

[14] Baragetti A, Da Dalt L, Moregola A, Svecla M, Terenghi O, Mattavelli E, et al. Neutrophil aging exacerbates high fat diet induced metabolic alterations. Metabolism 2023;144:155576. https://doi.org/10.1016/j.metabol.2023.155576.

[15] Wierer M, Prestel M, Schiller HB, Yan G, Schaab C, Azghandi S, et al. Compartment-resolved proteomic analysis of mouse aorta during atherosclerotic plaque formation reveals osteoclast-specific protein expression. Mol Cell Proteomics 2018;17:321–34. https://doi.org/10.1074/mcp.RA117.000315.

[16] Pulakazhi Venu VK, Uboldi P, Dhyani A, Patrini A, Baetta R, Ferri N, et al. Fibronectin Extra domain A stabilises atherosclerotic plaques in apolipoprotein E and in LDL-receptor-deficient mice. Thromb Haemost 2015;114:186–97. https://doi.org/10.1160/TH14-09-0790.

[17] Svecla M, Da Dalt L, Moregola A, Nour J, Baragetti A, Uboldi P, et al. ASGR1 deficiency diverts lipids toward adipose tissue but results in liver damage during obesity. Cardiovasc Diabetol 2024;23:42. https://doi.org/10.1186/s12933-023-02099-6.

[18] Tomas L, Edsfeldt A, Mollet IG, Perisic Matic L, Prehn C, Adamski J, et al. Altered metabolism distinguishes high-risk from stable carotid atherosclerotic plaques. Eur Heart J 2018;39:2301–10. https://doi.org/10.1093/eurheartj/ehy124.

[19] Sun J, Singh P, Shami A, Kluza E, Pan M, Djordjevic D, et al. Spatial transcriptional mapping reveals site-specific pathways underlying human atherosclerotic plaque rupture. J Am Coll Cardiol 2023;81:2213–27. https://doi.org/10.1016/j.jacc.2023.04.008.

[20] Robinson MD, McCarthy DJ, Smyth GK. edgeR : a bioconductor package for differential expression analysis of digital gene expression data. Bioinformatics 2010;26:139–40. https://doi.org/10.1093/bioinformatics/btp616.

[21] Johnson WE, Li C, Rabinovic A. Adjusting batch effects in microarray expression data using empirical Bayes methods. Biostatistics 2007;8:118–27. https://doi.org/10.1093/biostatistics/kxj037.

[22] Korotkevich G, Sukhov V, Budin N, Shpak B, Artyomov MN, Sergushichev A. Fast gene set enrichment analysis. Preprint 2016. https://doi.org/10.1101/060012.

 © 2025 The Author(s). Published by Elsevier GmbH. This is an open access article under the CC BY-NC-ND license (http://creativecommons.org/licenses/by-nc-nd/4.0/).